Ultrasonics 111 (2021) 106312

Contents lists available at ScienceDirect

Ultrasonics

journal homepage: www.elsevier.com/locate/ultras

Deconvolution of ultrasonic signals using a convolutional neural network

Arthur Chapon [a], Daniel Pereira [a], Matthew Toews [b], Pierre Belanger [a,*]

[a] Department of Mechanical Engineering, École de technologie supérieure, 1100 rue Notre-Dame Ouest, Montréal, Québec H3C 1K3, Canada
[b] Department of Systems Engineering, École de technologie supérieure, 1100 rue Notre-Dame Ouest, Montréal, Québec H3C 1K3, Canada

ARTICLE INFO

Keywords:
Ultrasonic testing
Axial resolution
Time-of-flight
Deconvolution
Convolutional neural network

ABSTRACT

Successfully employing ultrasonic testing to distinguish a flaw in close proximity to another flaw or geometrical feature depends on the wavelength and the bandwidth of the ultrasonic transducer. This explains why the frequency is commonly increased in ultrasonic testing in order to improve the axial resolution. However, as the frequency increases, the penetration depth of the propagating ultrasonic waves is reduced due to an attendant increase in attenuation. The nondestructive testing research community is consequently very interested in finding methods that combine high penetration depth with high axial resolution. This work aims to improve the compromise between the penetration depth and the axial resolution by using a convolutional neural network to separate overlapping echoes in time traces in order to estimate the time-of-flight and amplitude. The originality of the proposed framework consists in its training of the neural network using data generated in simulations. The framework was validated experimentally to detect flat bottom holes in an aluminum block with a minimum depth corresponding to $\lambda/4$.

1. Introduction

In the metal forming and composite manufacturing industries, flaws detection close to interfaces is critical. A successful early detection of these flaws can reduce the probability of failure during the useful life of manufactured components. Ultrasonic testing (UT) is commonly used to quality control such components. In the inspection of thick components and/or highly attenuative materials (such as cast iron or composite), a compromise between the penetration depth and the axial resolution must be reached. It may therefore become difficult to detect flaws in close proximity or near the boundaries of the part under inspection. Increasing the frequency reduces the wavelength and therefore leads to an increase in the axial resolution. However, attenuation increases as the frequency increases, and consequently, the maximum propagation depth reduces. The duration of the transmitted wave packet associated with the bandwidth of the transducers also plays an important role in the axial resolution. For a transducer with an infinite bandwidth emitting a single cycle pulse waveform, the axial resolution is half a wavelength [1]. In practice, piezoelectric transducers have a limited bandwidth, which restricts the minimum duration of the transmitted pulse to a few cycles, and consequently, reduces the axial resolution. Therefore, achieving a satisfactory axial resolution is a function of the transducer bandwidth, the attenuation of the inspected medium, and the propagation distance.

Hoseini et al. [2] showed that combining the Hilbert transform and a quasi-maximum likelihood method could be efficient for measuring the Time-of-Flight (ToF) and locating experimental reflectors in signals with a signal-to-noise ratio (SNR) as low as 5 dB. In their work, the location accuracy was better than when using the cross-correlation method. However, the separation of two reflectors in close proximity was not covered. The separation of two overlaping wave packets is critical to increasing the axial resolution. In this context, the application of deconvolution methods to distinguish signals that are overlapped has been extensively studied in geophysics [3] and ultrasonic NDT [4]. Researchers in geophysics are interested in extracting the ToF and amplitudes of overlapping seismic events. According to Crump [5], the deconvolution may be used to separate echoes to estimate the positions of emissions, but the difficulty in dealing with waveshape-changing phenomena, including noise and overlapping echoes, was noted. Deconvolution algorithms such as the least-squares deconvolution [6] or the autoregressive spectral extrapolation [7] suffer from various limitations: (1) they require a priori knowledge of the interface reflectivity inside the propagating medium as well as information regarding the path of multiple reflections; (2) they are very sensitive to structural and electronic noise. In [4], blind deconvolution techniques were applied to address this problem by adding iterative filters. These filters were able to

* Corresponding author.
E-mail address: pierre.belanger@etsmtl.ca (P. Belanger).

https://doi.org/10.1016/j.ultras.2020.106312
Received 19 November 2019; Received in revised form 16 September 2020; Accepted 19 November 2020
Available online 26 November 2020

deconvolve with a weak knowledge of the echo pattern. Convolutive filters (e.g., the Wiener filter) have also been developed to improve the robustness of deconvolution against noise [8,9].

In UT, the ToF measurement of strongly overlapping wave packets in noisy signals was also studied. Soussen et al. [10] proposed a sparse deconvolution method capable of picking more than 6 successive reflections in a simulated 2 mm aluminum plate. The wavelength was greater than the plate thickness and the pulse was a 3-cycle Hann windowed toneburst, thus leading to overlapping echoes. The results showed a reduction in performance when the SNR was synthetically reduced from 20 dB to 10 dB. Cicero et al. [9] encountered another problem with deconvolution in structural health monitoring (SHM). Their simulation study showed the potential of the optimal Wiener filter to deal with overlapped signals. The deconvolutional algorithm was able to separate two completely overlapped and noisy 4-cycle waveforms in a metal plate. The performance of the method was satisfactory when using simulated data, but the experimental implementation was disappointing. This poor performance was associated with the narrow bandwidth of transducers, which extends the temporal size of the echo patterns. Various methods have been proposed in the field of ultrasonic tomography for the estimation of the ToF of overlapping wave packets [11–13], with limited success.

Convolutional neural networks (CNN) could overcome the problem of transduction bandwidth by learning the shape of overlapping signals in the time domain. A CNN contains several layers and adapts the filters by learning the waveforms. The classification of ultrasonic testing signals using CNN has already been demonstrated. Virupakshappa et al. [14] used a CNN to detect the presence or the absence of flaws, and demonstrated the ability of neural networks to process signals in noisy situations. In their case, the signal was pre-processed by a discrete wavelet transform. Munir et al. [15] also demonstrated that CNN were able to classify defects in welds, even in the presence of noise. Training a CNN requires a large amount of data to achieve acceptable performances. Large sets of experimental measurements are difficult to generate because of the cost associated with preparing samples. Data augmentation solutions exist, and allow to compensate for the small amount of samples through minor geometric changes such as translation, rotation, etc. [16]. Munir et al. [15] implemented data augmentation through time shifting of the A-Scans and the addition of white Gaussian noise representing electronic noise. Data augmentation methods are particularly interesting when it is difficult to generate a high fidelity simulated dataset.

As mentioned above, this paper aims to demonstrate the concept of employing a CNN trained using simulated data to deconvolve experimental A-Scans even when wave packets are strongly overlapping. The aim of the CNN is to retrieve both the time of arrival and amplitude relative to the backwall in a A-Scan. Both the ToF and the amplitude are typically required in sizing defects. Experimental measurements are used to validate the performance of the proposed approach. The paper begins with the materials and methods section describing the finite element model, the CNN and its training, followed by the experimental procedure. The presentation of the results is then followed by discussions. Finally, conclusions are drawn.

2. Materials and methods

2.1. Finite element simulated dataset

To satisfactorily train neural networks, a large amount of data is required. A convenient way to generate this data is to use simulations rather than experiments. In this paper, the dataset was generated using GPU-accelerated finite element (FE) simulations using Pogo FEA [17]. A 2D plane strain model was used to simulate an aluminum block with flaws near the backwall. The aluminum material properties were $E = 72.5$ GPa, $\upsilon = 0.33$, $\rho = 2706$ kg/m^3. The model was discretized at 30 elements per wavelength using linear square elements. In the simulation set, the cases were all different in order to avoid unbalancing the training. To this end, a matrix of parameters containing random sizes and reflector positions was generated. These parameters were used to generate FE models whose schematic is presented in Fig. 1.

Absorbing boundaries [18], in light grey in Fig. 1, were added to both sides and to the bottom boundary of the model. Their aim was to reduce the size of the mesh in the x-direction and to avoid reverberations between a reflector and the backwall. In this study, the reflectors (shown in white) were flat, and were generated through element suppression, and therefore correspond to voids. Their thickness corresponded to one layer of elements. The black dots at the top of the model show the nodes used for the excitation. The positions (X_1, X_2, Y_1 and Y_2) and lengths (L_1 and L_2) of the two reflectors were random, while L_2 was always greater than L_1. The positions and lengths of the reflectors were stored in memory to be used during the supervised learning of the network.

When using a simulated dataset to train a CNN, the fidelity of the simulations is paramount. On top of using a high number of elements per wavelength and the appropriate time step it was found that the transducer bandwidth used in the experiments was essential. Therefore, an initial experimental measurement in an aluminum block was used to estimate the bandwidth of the acquisition chain used in the experimental validation of the method (see Section 2.4). The average time trace obtained in this experiment was used as the input signal of the finite element simulations.

A set of 2000 simulated A-Scans were computed in under an hour for the training of the CNN.

2.2. Architecture of the CNN

Among the diversity of artificial neural networks, the CNN caught attention because of its ability to take into account the temporal organization of an A-Scan. Moreover, this type of neural network is the most commonly used in pattern recognition [19]. CNN have been studied in the classification or detection of reflectors in ultrasonic signals [14]. This paper is interested in using a CNN to retrieve the time of arrival as well as the amplitude of wave packets relative to the backwall. The relative amplitude to the backwall is important in sizing methods such as the 6 dB drop method [20]. It was therefore decided to formulate the problem as a regression. This method appeared more suitable to estimate the amplitude response at each time index in an A-Scan compared to a classification approach. As the temporal size of the echo pattern is known with the parameters of the simulation, the size of the region of interest (ROI) can be computed using equation (1):

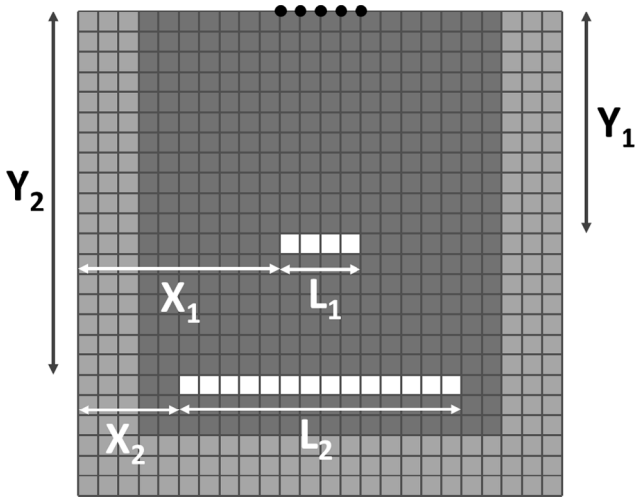

Fig. 1. Schematic of the FE model.

$$ROI = \frac{N_{cycle} \times f_{sampling}}{f_{signal}} \quad (1)$$

In order to reduce the computational complexity and the number of unknowns during the training phase, the input layer of neurons can be adapted to the size of the ROI. Since the duration of an echo is known, the number of neurons in the first layer of the CNN is adapted to this size. Adding more neurons would not provide more information, whereas using less would mean not all the information available is used. The kernel of the first convolutional layer was set to cover the full length of ROI.

The estimation of the amplitude of a known echo pattern inside a wave packets in an A-Scan can be thought of as a regression problem. It was assumed that the output of the CNN is stronger at time index of a reflector than elsewhere. A proportional output imposes the usage of ReLU, eLU or other linear-when-positive activation functions rather than the sigmoid or the hyperbolic tangent [21]. Moreover, since the interest is in detecting direct and hard skips, negative outputs are not expected. Therefore, the most adapted activation function was chosen as the ReLU.

A dropout layer with a rate of 0.5 was set between both convolutional layers. The expected effect of this layer is to avoid overfitting [22], or specialization of the CNN in the simulation domain. The last 1x1 convolutional layer synthesized the results from all channels. The architecture of the CNN is shown in Fig. 2. The keras library was used in the present study to design and train the neural network.

The learning dataset comprised 2000 simulated A-Scans. 400 (20%) of them were used as a validation set to evaluate the performance during the learning. Another batch of 50 simulations (2.5%) was used to test the performances of the CNN. All the other A-Scans (1550) were used for the supervised training.

A stochastic gradient descent was used to minimize the mean square error loss function. The learning rate was initially 0.005, and decreased logarithmically with the epochs. The learning stopped when 30,000 epochs were computed. Fig. 3 shows the evolution of the loss function; an asymptote was reached from approximately the 12,000th epoch. The gap between the scores of the training and validation sets was still narrow enough to suggest that overfitting was avoided.

2.3. Training the CNN with simulations

A typical A-Scan (Fig. 4) is a time vector containing the temporal position and amplitude of echoes as well as some noise. The A-Scan is the convolution of the input signal (p) with the position of the reflectors and

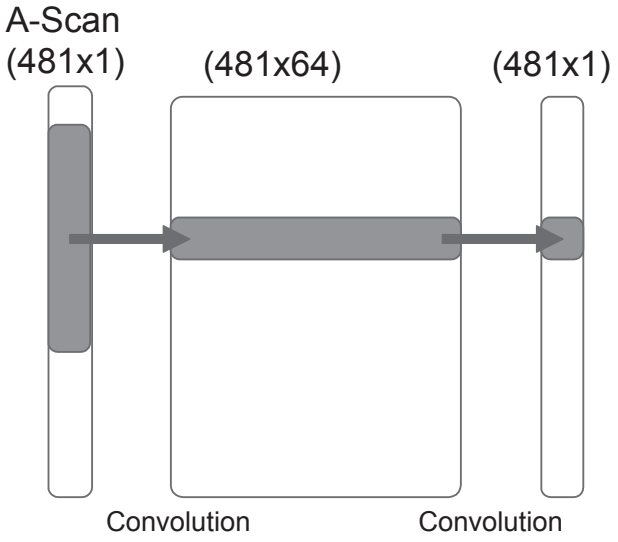

Fig. 2. Schematic of the network architecture.

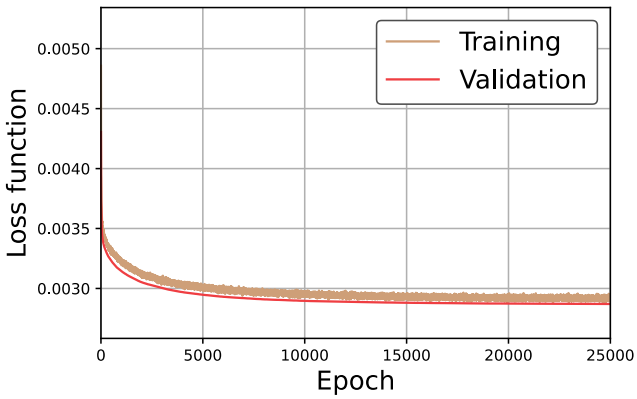

Fig. 3. Learning curve and loss function as a function of epoch.

their amplitude (g) plus some noise (n). In this paper, the aim of the CNN is to recover the position of the reflectors (g) from the A-Scan.

The steps to format the data into a training set are summarized in Fig. 5. As mentioned previously, only five experimental measurements were used in the preparation of the simulated training set. The experimental noise, the experimental echo pattern and the speed of sound were extracted from them.

As the CNN work as a waveform filter in the time domain, the echo patterns from simulations and experiments must be similar. Hence, five preliminary experimental measurements were made to extract a back-wall echo waveform. The approach was therefore close to a non-blind deconvolution method. After the simulations were completed, the simulated A-Scans were downsampled to fit the sampling frequency of the experiments. The downsampling step also had the benefit of reducing the size of the input data, thus reducing the training time. A typical simulated A-Scan next to a experimental A-Scan is presented in Fig. 6.

Noise is commonly added to the simulations when training or testing CNN [15] to simulate structural, systems or electronic noise, and to introduce a more random part in simulated and experimental signals. To that end, experimental noise was extracted from the five preliminary experimental measurements in sections of the A-Scans where no reflectors were present. All the noise was then concatenated into a single vector. A weighted random section of the noise was added to each simulated A-Scan, as shown in Fig. 7. This method enabled the use of typical noise acquired in experiments. The noise takes into account the bandwidth of the entire acquisition chain, including the transducer, the acquisition card and all unwanted filtering. Three learning batches of 2000 simulations were generated: (1) free from any noise, (2) with an SNR of 20 dB, and (3) with an SNR of 5 dB. The effect of noise on the performance of the CNN could therefore be studied. The amplitude of the added noise A_{noise} was set using Eq. (2) as a function of the signal amplitude A_{signal}:

$$A_{noise} = A_{signal}.10^{\frac{-SNR_{dB}}{20}} \quad (2)$$

Finally, the simulated signals were normalized to the amplitude of the strongest reflector in order to avoid the saturation of the activation functions and to get a more homogeneous dataset. In Fig. 8, the grey line shows a simulated A-Scan after adaptation, and the brown line is the expected output from the CNN. The spikes in the brown line correspond to the beginning of the arrival of the signals from the two reflectors. Throughout the article, the amplitude of the expected signal is set to unity. Indeed, determining the amplitude contribution of each reflector in an overlaping wavepacket of an experimental signal is outside the scope of this paper.

Fig. 4. A typical A-Scan (s) with its three components: (g) the position of the reflectors, (p) the input signal and (n) the noise.

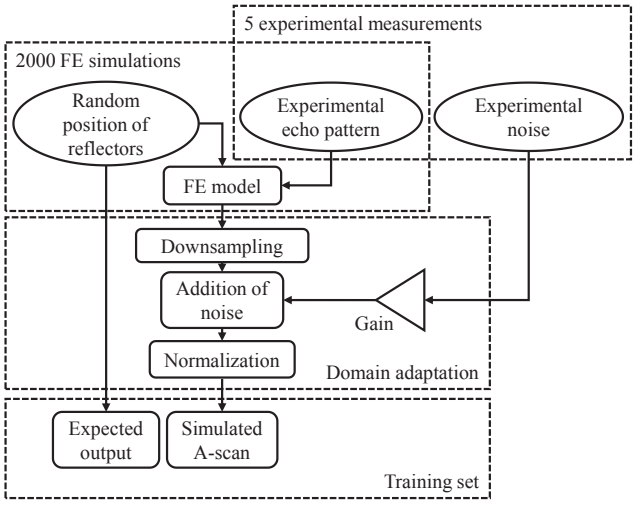

Fig. 5. Preparation of the simulated training batch for the CNN.

2.4. Experimental setup

An aluminum block was used to assess the performance of the framework to identify the ToF of reflectors. 23 flat-bottom holes (FBH) were machined with depths ranging from 0.69 mm to 13.77 mm. The diameter of the FBH was 8 mm. The aim of the experiments was to distinguish the top of the FBH from the backwall. The performance of the CNN was evaluated as a measure of its ability to identify reflectors as well as the minimum resolvable distance between the top of an FBH and the backwall of the block. An Olympus single-element probe V125-RM with a center frequency of 2.25 MHz was used in a pulse-echo arrangement. The 3-cycle Hann windowed toneburst was generated using a Verasonics Vantage 64LE data acquisition system. The sampling frequency was set to 25 MHz. The aluminum block and the experimental setup are shown in Fig. 9.

Fig. 10 shows five experimental reflections obtained from the backwall of an aluminum block and the frequency spectrum of the averaged signals. The backwall echo pattern depends on the rugosity of the part, the ultrasonic couplant quantity or the hand-pressure applied on the probe during the measurement. The average time trace obtained in this experiment was considered as the most probable echo to detect. This signal was used as the input signal of the finite element simulations as well as to extract typical experimental noise.

After the CNN training, a series of measurements were acquired to test the algorithm in laboratory conditions. 48 A-Scans – 2 for each position above the FBH and 2 others above the backwall – were stored. The measured A-Scans were normalized following the same procedure as for the simulated A-Scans and directly passed through the CNN.

3. Results

The experimental measurements were repeated twice for 23 FBH and

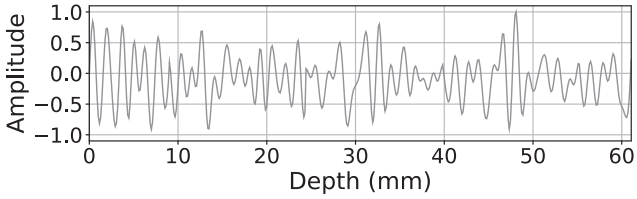

Fig. 7. Noise extracted from the preliminary experimental measurements, after normalization.

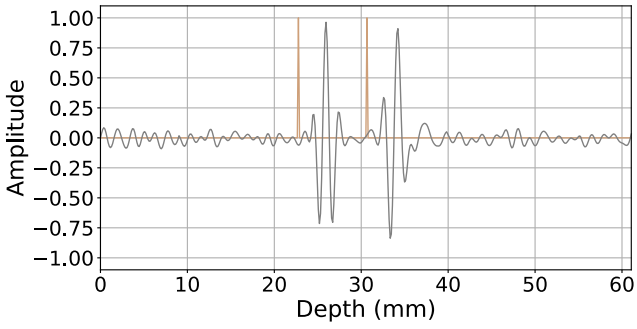

Fig. 8. Simulated A-Scan used for CNN training after domain adaptation. The expected output corresponds to spikes at the beginning of the signals of interest.

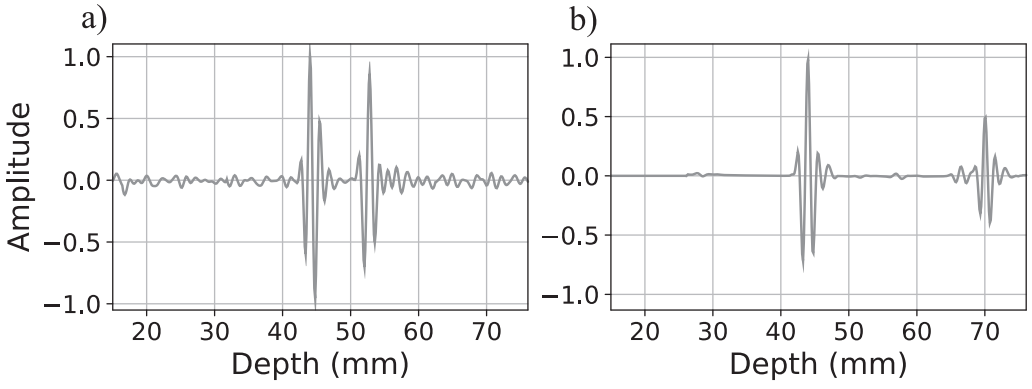

Fig. 6. Typical raw data a) an experimental A-Scan and b) a FE simulated A-Scan.

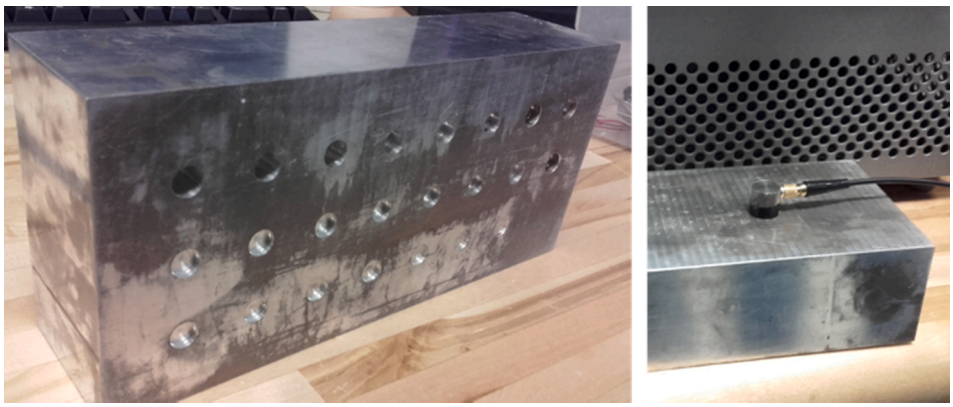

Fig. 9. Aluminum block with different FBH depths and the Olympus V125-RM probe.

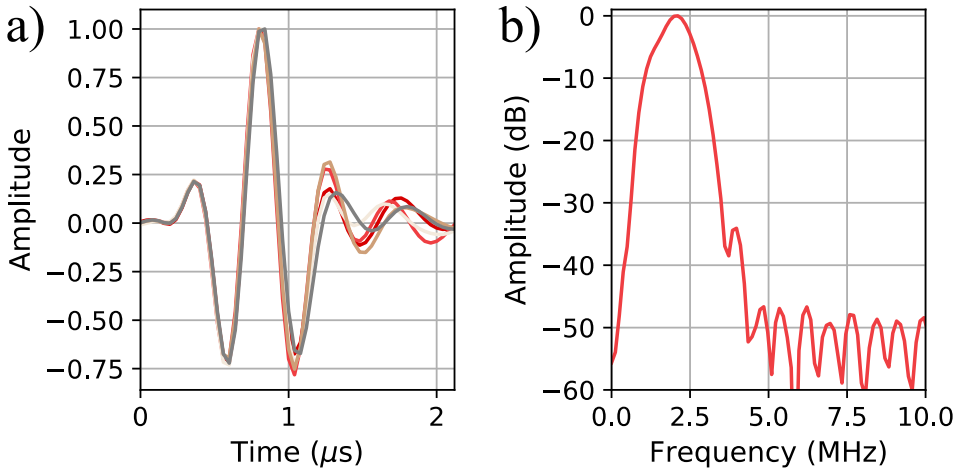

Fig. 10. Five reflections from the backwall of an aluminum block using an Olympus V125-RM probe centered at 2.25 MHz: (a) 5 time traces and (b) the averaged frequency spectrum.

1 position without defect. Hence, the CNN had to locate 94 reflectors (2 per measurement with an FBH and only 1 when there was no FBH) in the 48 experimental A-Scans. These signals were passed through the CNN without any pre-filtering.

When compiling the results, an FBH or the backwall was considered detected if it was located within a window of five sample indices from the expected position. Five sample indices at 25 MHz corresponded to 0.2 μs or 1.3 mm in the aluminum block. If the location was outside this narrow window, it was considered either a false detection or a non-detected reflector. An amplitude threshold of 10% was used along the amplitude axis; this value was set using the 50 simulations of the performance test batch. Indications from the CNN below this threshold were ignored.

Firstly, the neural network was applied on the raw experimental A-Scans. The SNR on the raw A-Scans was approximately 40 dB. The CNN trained without noise was used for this case. The results are summarized in Table 1. All the reflectors were detected, with no false detection recorded. Fig. 11 shows an example of the result obtained on the shallowest FBH (depth of 0.69 mm).

Table 1
Results of the CNN deconvolution on the raw experimental A-Scans.

	True	False	Total
Detection	Reflector detections: 94 (100%)	False detection: 0 (0.0%)	94
Reflector	Reflectors detected: 94 (100%)	Non-detected reflectors: 0 (0.0%)	94

The top of the FBH is slightly misplaced in Fig. 11, but still within the acceptable range of 5 indices, or 1.3 mm in our experimental case. Altough the amplitude of the CNN output was weak, it was above the 10% threshold. Fig. 12 shows the location error as a function of the distance between the reflectors for the CNN trained using simulated data and tested on raw experimental measurements.

In order to verify the performance in a less favorable scenario, the noise level of the experimental A-Scans was synthetically increased to reach an SNR of 20 dB and 5 dB. The method to add the noise was the same as in the simulations.

The results for the SNR of 20 dB are presented in Table 2. The SNR of the training set for this case was also 20 dB. In this case, only the two

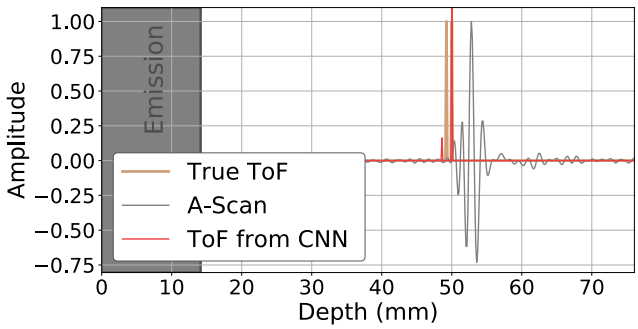

Fig. 11. Location of reflectors in a raw A-Scan for an FBH with a depth of 0.69 mm.

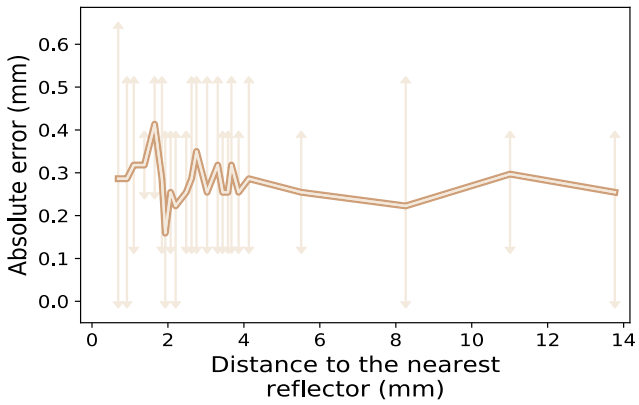

Fig. 12. Location error as a function of the distance to the nearest reflector.

measurements on the shallowest FBH were unsuccessful. Encouragingly, the CNN was right in all other cases, and did not give any false detection.

When the SNR was 5 dB, the presence of false detection increased significantly, as shown in Table 3. The SNR of the training set for this case was also 5 dB. 8% of the detections were false, and only 85.1% of the reflectors were detected. As for when the SNR was 20 dB, the shallowest FBH were not detected. The other cases of non-detected reflectors or false detections were not linked to the distance between two reflectors. Fig. 13 shows a successful example, with an SNR of 5 dB when the depth of the FBH was 0.96 mm. This was the shallowest FBH that the CNN was able to distinguish from the backwall when the SNR was set to 5 dB.

A threshold of 10% of the maximum amplitude was used to avoid false detection and ensure that 6 dB drop method could be used to size FBH. Other threshold values were tested when the CNN was trained and tested with the 5 dB SNR. Initially, the threshold was set using only simulations to optimize the number of true detections. Table 4 shows the number of false detections and detected reflectors for three different thresholds (1%, 10% (original value), and 20%). A threshold value of 1% clearly led to many false detections, but also increased the number of detected reflectors. When the threshold increased to 20%, the number of detections – true and false – was reduced.

The effect of noise on the CNN was also evaluated and the results are summarized in Table 5. The table shows the reflectors detected and the false detections for each case (Raw data – SNR = 40 dB, SNR = 20 dB and SNR = 5 dB) using the 3 different trainings (CNN trained without noise, SNR = 20 dB, and SNR = 5 dB).

The estimation of the amplitude of the signal reflected from a FBH relative to the amplitude of the backwall wave packet was successful in all cases when the wave packets were separated in the time domain. However, when the wave packets were overlapping the results were not consistent. The reasons for this inconsistency are discussed in the following section.

4. Discussion

When using the raw experimental data, the CNN was able to separate the echoes for an FBH with a depth of only 0.69 mm. In this case, due to the pulse-echo propagation, this length corresponds to a separation distance of λ/2 at 2.25 MHz in the aluminum block. Moreover, on the raw experimental data, the CNN correctly identified all reflectors, with no false detection. As the raw experimental A-Scans had an SNR of approximately 40 dB, a standard deconvolution may provide similar results. Fig. 14 compares the proposed CNN framework with the least squares deconvolution. Fig. 14(a) shows a comparison of the raw experimental data with a 0.96 mm FBH, while Fig. 14(b) shows the same comparison when noise was added to reach an SNR of 20 dB. The deconvolved signals were filtered in the bandwidth of the original signal. On the raw experimental signals, the deconvolution and the CNN provide similar results. However, when the SNR was reduced to 20 dB, the deconvolution had multiple secondary lobes, leading to difficulty in the interpretation of the results. In the presence of noise, even relatively weak, the proposed CNN framework appears to perform better than the least-squares deconvolution.

Fig. 12 showed that the accuracy of the true detection was approximately 0.3 mm and remained constant for any distance between the reflectors. Hence, the proximity of reflectors did not affect the accuracy of the CNN.

When the SNR was reduced to 20 dB, the axial resolution achieved by the CNN was reduced and the shallowest FBH was not detected. Hence, the CNN was able to distinguish reflectors when the FBH depth was 0.96 mm, corresponding to 0.65λ in an aluminum block at 2.25 MHz.

When the SNR was reduced to 5 dB, the CNN again successfully detected the FBH with a depth of 0.96 mm. The reliability of the CNN was, however, dramatically reduced, with a 7.5% false detection and 14.9% of reflectors missed. Again, no relationship was found between the detected reflectors and their proximity in this case. Hence, the presence of significant noise was a greater problem than the overlapping echoes. Two reasons were identified to explain the number of false detections: 1) the noise was added in the bandwidth of the transducers, and

Table 2
Results of the CNN deconvolution on the experimental A-Scans with the noise synthetically increased to reach an SNR of 20 dB.

	True	False	Total
Detection	Reflector detections: 92 (100%)	False detection: 0 (0.0%)	92
Reflector	Reflectors detected: 92 (97.9%)	Non-detected reflectors: 2 (2.1%)	94

Table 3
Results of the CNN deconvolution on the experimental A-Scans with the noise increased to reach an SNR of 5 dB.

	True	False	Total
Detection	Reflector detections: 81 (92%)	False detections: 7 (8.0%)	88
Reflector	Reflectors detected: 80 (85.1%)	Non-detected reflectors: 14 (14.9%)	94

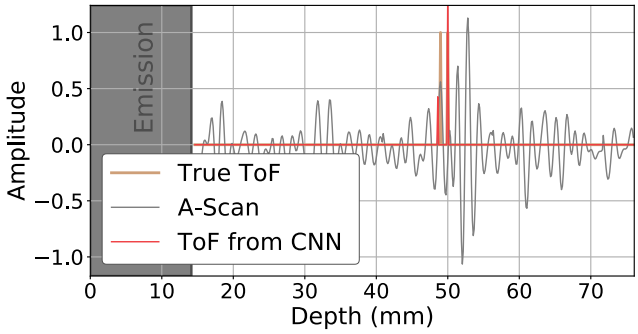

Fig. 13. Example of an FBH detected with an SNR of 5 dB. The FBH depth was 0.96 mm.

Table 4
Effect of the threshold value on the deconvolution of the experimental measurements with an SNR of 5 dB.

Threshold	1%	10%	20%
False detections	42	7	4
Detected reflectors	90	80	78
Total:	**132**	**87**	**82**

Table 5
Results of the three CNN tested with experimental measurements with different added noise values.

	CNN – Trained Without Noise Added		CNN – Trained with SNR = 20 dB		CNN – Trained with SNR = 5 dB	
	Reflectors Detected	False Detections	Reflectors Detected	False Detections	Reflectors Detected	False Detections
SNR = 40 dB (raw data)	100%	0%	93.7%	4.3%	92.6%	2.12%
SNR = 20 dB	92.6%	7.4%	97.9%	0%	93.6%	0%
SNR = 5 dB	89.4%	12.8%	90.4%	10.7%	85.1%	7.45%

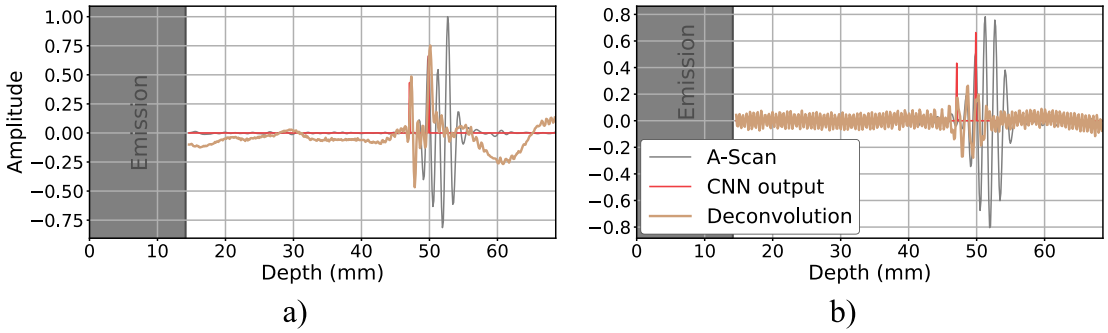

Fig. 14. Comparison of the proposed CNN framework with the least-squares deconvolution. The FBH had a depth of 1.65 mm: (a) Raw experimental A-Scans, and (b) SNR reduced to 20 dB.

therefore, in some instances, the noise pattern was similar to an echo pattern, and 2) some reflectors were slightly misplaced and dropped out of the acceptable window, and they were not detected, and were considered as false detections. Table 4 showed that the threshold did have an effect on the performance of the CNN. When the SNR was at 5 dB, the initial threshold (10%) led to non-detected reflectors (see Fig. 15 (a)). Hence, with a low threshold, the amount of detected reflectors would increase. However, the number of false detections would also increase. A tradeoff is made to keep an acceptable true location rate and false detection rate. The tradeoff between a threshold of 10% and 20% is more questionable, depending on the most unfavorable case (i.e., false detections or reflectors missed). In any case, the choice of the threshold value may have a strong impact on the success of the proposed framework.

The estimation of the amplitude of overlapping echoes is key to successful FBH sizing using the 6 dB drop. However, in the experimental validation the alignment along the x-axis between the probe and the defect was difficult to measure. Therefore, the amplitude prediction obtained from the CNN could not be validated and appeared to be inconsistent. This inconsistency is not necessarily due to the performance of the CNN but could be because of poor alignment of the probe over the FBH. However, when the wave packets were not overlapping corresponding to the deeper FBH, the amplitude of the wave packet predicted by the CNN were in good agreement with the amplitude measured directly on the A-Scan.

One of the limitations of the method presented in this paper is the low number of reflectors present in a single A-Scan. A second study should consider more reflectors in order to open this method up to other applications, such as ultrasonic guided wave structural health monitoring or ultrasonic tomography, where several modes propagate. Another limitation of the proposed method is the need to retrain the CNN when measurement parameter, such as the transducer bandwidth, change. In such cases, running the simulations would take a few hours, and the training, several minutes.

5. Conclusion

This paper investigated the use of CNN for the deconvolution of A-Scans. The CNN was trained using simulations. However, the simulations were generated from 5 experimental measurements in order to extract the bandwidth of the transducers, the speed of sound in the material, and a typical measurement noise. Using GPU-accelerated FE simulations, 2000 A-Scans were generated in only a few hours. The trained CNN was then used to deconvolve experimental A-Scans acquired on an aluminum block with FBH. On the raw experimental measurements, the axial resolution was 0.5λ, with no false detection and no reflectors missed. When the noise was artificially increased to 20 dB, the axial resolution was reduced to 0.65λ, with no false detection, and only the shallowest FBH missed. When the noise was artificially increased to 5 dB, the axial resolution remained at 0.65λ, but the number

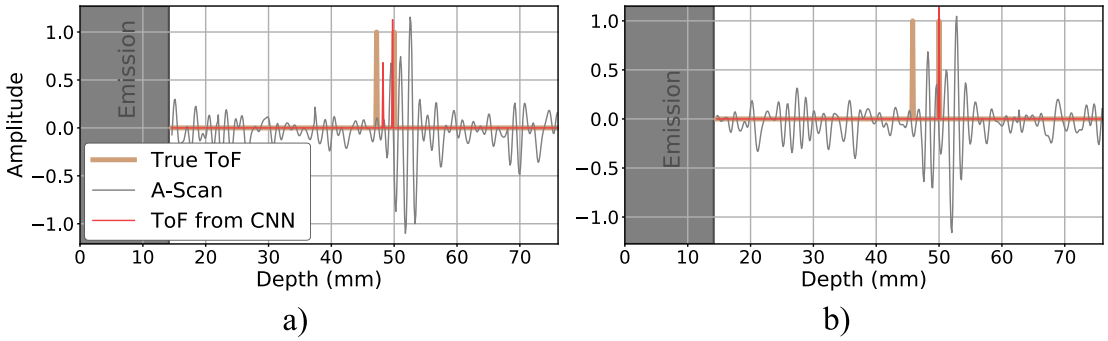

Fig. 15. Examples of (a) misplaced and (b) non-detected reflectors with a 5 dB noise.

of false detections and missed reflectors increased dramatically. Overlapping wave packets is a common problem across all fields of application of ultrasonic waves and therefore the method proposed in this paper could be further developed in geophysics or medical ultrasound.

Declaration of Competing Interest

The authors declare that they have no known competing financial interests or personal relationships that could have appeared to influence the work reported in this paper.

Acknowledgments

The authors would like to thank Nvidia for providing them with an Nvidia Quadro P6000 graphics card for their GPU simulations. They would also like to thank the Natural Sciences and Engineering Research Council of Canada for funding this project under the oN DuTy! program. Data and codes used in this paper are available at https://pulets.ca/open-data/S0041624X2030247X.

References

[1] D. Dance, S. Christofides, A. Maidment, I. McLean, K. Ng, Diagnostic radiology physics, Int. Atomic Energy Agency, 2014, p. 299.
[2] M.R. Hoseini, X. Wang, M.J. Zuo, Estimating ultrasonic time of flight using envelope and quasi maximum likelihood method for damage detection and assessment, Measurement 45 (8) (2012) 2072–2080, https://doi.org/10.1016/j.measurement.2012.05.008.
[3] A. Jurkevics, R. Wiggins, A critique of seismic deconvolution methods, Geophysics 49 (12) (1984) 2109–2116, https://doi.org/10.1190/1.1441627.
[4] G. A. Guarneri, D. R. Pipa, F. Neves, L.V. de Arruda, A blind deconvolution approach to discontinuity location and characterization in ultrasonic nondestructive testing, in: 2017 25th European Signal Processing Conference (EUSIPCO), 2017, IEEE, pp. 2496–2500, doi: https://doi.org/10.23919/EUSIPCO.2017.8081660.
[5] N.D. Crump, Techniques for the deconvolution of seismic signals, in: 1975 IEEE Conference on Decision and Control including the 14th Symposium on Adaptive Processes, 1975: IEEE, pp. 2–8.
[6] E.A. Robinson, S. Treitel, Geophysical signal analysis, Soc. Explor. Geophys. (2000).
[7] J. Chen, X. Bai, K. Yang, B.-F. Ju, An ultrasonic methodology for determining the mechanical and geometrical properties of a thin layer using a deconvolution technique, Ultrasonics 53 (7) (2013) 1377–1383, https://doi.org/10.1016/j.ultras.2013.04.006.
[8] S.H. Bickel, D. Martinez, Resolution performance of Wiener filters, Geophys. 48 (7) (1983) 887–899, https://doi.org/10.1190/1.1441517.
[9] T. Cicero, P. Cawley, F. Simonetti, S. Rokhlin, Potential and limitations of a deconvolution approach for guided wave structural health monitoring, Struct. Health Monit. 8(5) (2009) 381–395, doi: https://doi.org/10.1177%2F1475921709102086.
[10] C. Soussen, J. Idier, E. Carcreff, L. Simon, C. Potel, Ultrasonic non destructive testing based on sparse deconvolution, J. Phys.: Conf. Series 353(1) 2012. IOP Publishing, p. 012018, doi: https://doi.org/10.1088/1742-6596/353/1/012018.
[11] C. Li, L. Huang, N. Duric, H. Zhang, C. Rowe, An improved automatic time-of-flight picker for medical ultrasound tomography, Ultrasonics 49 (1) (2009) 61–72.
[12] T. Falardeau, P. Belanger, Ultrasound tomography in bone mimicking phantoms: simulations and experiments, J. Acoust. Soc. Am. 144 (5) (2018) 2937–2946.
[13] L. Espinosa, J. Bacca, F. Prieto, P. Lasaygues, L. Brancheriau, Accuracy on the time-of-flight estimation for ultrasonic waves applied to non-destructive evaluation of standing trees: a comparative experimental study, Acta Acustica United Acustica 104 (3) (2018) 429–439.
[14] K. Virupakshappa, M. Marino, E. Oruklu, A multi-resolution convolutional neural network architecture for ultrasonic flaw detection, in: 2018 IEEE International Ultrasonics Symposium (IUS), 2018: IEEE, pp. 1–4, doi: https://doi.org/10.1109/ULTSYM.2018.8579888.
[15] N. Munir, H.-J. Kim, J. Park, S.-J. Song, S.-S. Kang, Convolutional neural network for ultrasonic weldment flaw classification in noisy conditions, Ultrasonics 94 (2019) 74–81, https://doi.org/10.1016/j.ultras.2018.12.001.
[16] I. Virkkunen, T. Koskinen, O. Jessen-Juhler, J. Rinta-Aho, Augmented ultrasonic data for machine learning, 2019, arXiv preprint arXiv:1903.11399.
[17] P. Huthwaite, Accelerated finite element elastodynamic simulations using the GPU, J. Comput. Phys. 257 (2014) 687–707, https://doi.org/10.1016/j.jcp.2013.10.017.
[18] P. Rajagopal, M. Drozdz, E.A. Skelton, M.J. Lowe, R.V. Craster, On the use of absorbing layers to simulate the propagation of elastic waves in unbounded isotropic media using commercially available finite element packages, NDT and E Int. 51 (2012) 30–40.
[19] W. Rawat, Z. Wang, Deep convolutional neural networks for image classification: a comprehensive review, Neural Comput. 29 (9) (2017) 2352–2449.
[20] M.V. Felice, Z. Fan, Sizing of flaws using ultrasonic bulk wave testing: a review, Ultrasonics 88 (2018) 26–42.
[21] I. Goodfellow, Y. Bengio, A. Courville, Deep learning, MIT Press (2016).
[22] N. Srivastava, G. Hinton, A. Krizhevsky, I. Sutskever, R. Salakhutdinov, Dropout: a simple way to prevent neural networks from overfitting, J. Mach. Learn. Res. 15 (1) (2014) 1929–1958.